

1 **Supplemental Text: Additional Results**

2 **Brazelton et al. “Metabolic strategies shared by basement residents of the Lost City**
3 **hydrothermal field”**

4

5 **DETAILED COMPARISONS OF HYDROTHERMAL FLUID SAMPLES**

6 **Overview of sampling locations**

7 The present study included hydrothermal fluid samples from seven chimney locations: Camel
8 Humps, Sombrero, Marker 3, Marker C, Calypso, Marker 2, and Marker 8 (**Table 1**;
9 **Supplemental Table S1**). Several fluid samples collected from the Beehive chimney, where the
10 highest fluid temperatures have been measured, yielded only low-quality DNA sequences and
11 are not included in this study. The Sombrero site was sampled on two different ROV *Jason*
12 dives, and samples from the separate dives are labeled as Sombrero1 or Sombrero2 when
13 appropriate. Fluid samples collected from Markers C, 2, 3, and 8 were included in an early
14 microbial diversity study (1), but microbial diversity data from the other chimneys are reported
15 here for the first time.

16

17 **Markers 3 and C**

18 The strong similarity of community compositions from Markers 3 and C is remarkable
19 considering that fluids from Marker 3 were sampled at much lower temperatures (<20 °C) than
20 those from Marker C (up to 80 °C). Temperatures exceeding 55 °C were measured at Marker 3
21 during the same dive, but the temperatures of the fluid samples (i.e. measured in-line, during
22 sampling) used for DNA-based analyses were lower, most likely due to cooling of the fluids as
23 they exit the chimney. In addition, the pH, sulfate, sulfide, and magnesium levels of Marker 3
24 fluids are more similar to those of seawater, compared to Marker C fluids. These results suggest
25 that the cooler fluids venting from Marker 3 experience more dilution with ambient seawater

26 compared with the warmer fluids venting from Marker C, but that they share a common
27 subsurface source, which may explain the similar microbial compositions.
28
29 Marker 3 fluids were rich in metagenomic sequences classified as family *Methanosarcinaceae*,
30 which includes the dominant archaeal phylotype previously detected in Lost City chimneys (2–
31 4). Archaeal sequences were much more abundant in metagenomes than in the 16S rRNA
32 amplicon libraries. For example, *Methanosarcinaceae* is the most abundant family in Marker 3
33 metagenomic reads (1–2% of all reads and 20–21% of all reads that could be classified to the
34 family level by Kaiju; **Supplemental Table S3**), even though *Methanosarcinaceae* ASVs have
35 lower relative abundance than several bacterial ASVs in the same samples, suggesting a bias
36 against archaeal sequences in the ASV dataset.

37
38 Venting fluids collected near Markers C and 3 were particularly enriched in taxa representing
39 potential sulfate-reducing bacteria (SRB). *Thermodesulfovibrionia* and *Desulfotomaculum* ASVs
40 dominated these fluids, but they were much less abundant in the RNA fraction of the Marker C
41 sample (**Figure 3**). ASVs classified as *Desulfocapsa* were abundant in Marker 3 fluids, present
42 in the RNA fraction from Marker C, and absent in the DNA fraction from Marker C.
43 *Desulfobulbus* ASVs were absent in both Markers C and 3 except for the RNA fraction from
44 Marker C, and they were prevalent in Sombrero fluid samples. *Desulfobulbus* and *Desulfocapsa*
45 both belong to the family *Desulfobulbaceae*, which had 30-fold less coverage in Marker 3
46 metagenomes than *Methanosarcinaceae* and 8-fold less coverage than the *Nitrospiraceae*
47 family that includes *Thermodesulfovibrio* (**Supplemental Table S3**).
48

49 Marker 3 metagenomes were also distinctive in their high proportions of *Candidatus*
50 *Patescibacteria* (**Supplemental Figure S2**). Patescibacteria were rare in all samples except for
51 Marker 3 fluids, where they represented 33–36% of all classified sequences (**Supplemental**

52 **Table S3).** Hundreds of ASVs were classified as Patescibacteria (predominantly Paceibacteria
53 and Gracilibacteria), but they did not represent a large fraction of the counts in any of the fluid
54 samples (**Supplemental Table S2**).

55

56 **Camel Humps and Sombrero**

57 Fluids venting from Camel Humps contained a remarkably even distribution of ASVs that
58 included *Sulfurovum*, *Sulfurospirillum*, and *Thiomicrosrhabdus* at similar abundances as taxa
59 typically associated with ambient seawater (e.g. *Alteromonas*, *Roseobacter*, *Halomonas*). This
60 community composition strongly contrasts with that of Marker 3, even though both locations are
61 at the summit of the central Poseidon structure (**Figure 1**). Of the 100 ASVs most common in
62 Camel Humps fluids, 70 of these were significantly less abundant in Marker 3 fluids
63 (**Supplemental Table S2**). The differences between Camel Humps and Marker 3 cannot be
64 explained by mixing of the same hydrothermal fluid with ambient seawater because the bacteria
65 at Camel Humps belong to lineages associated with hydrothermal environments (e.g.,
66 *Sulfurovum*, *Sulfurospirillum*, *Thiomicrosrhabdus*), not ambient seawater. Moreover, the
67 temperatures measured during the sampling of Camel Humps fluids were higher than those of
68 Marker 3 fluids, which is the opposite of what would be expected if dilution by seawater had
69 been responsible for the observed trends. Instead, these results suggest a difference in the
70 subsurface source of the hydrothermal fluids venting from these locations. Although Marker 3
71 and Camel Humps are located next to each other, they are visually distinct chimney structures
72 that could potentially host fluids venting from distinct subsurface sources (**Supplemental Figure**
73 **S2**). Alternatively, the distinctive assemblage of taxa at Camel Humps may represent biofilm
74 communities that were flushed into nearby venting fluids, swamping the less dense organisms
75 derived from the subsurface. The two explanations are not mutually exclusive, and both indicate
76 that the fluids collected from Camel Humps during this study are not representative of the
77 subseafloor.

78

79 The Sombrero chimney is located on a ridge stretching from the main vent field toward the
80 eastern wall of the Atlantis Massif (**Figure 1**), and it was sampled on two separate ROV *Jason*
81 dives, with the second dive (Sombrero2) collecting fluids with higher temperatures and lower
82 sulfate concentrations than the first dive (Sombrero1) (**Table 1**). Despite these different
83 measurements at the time of sampling, the overall microbial composition was remarkably
84 consistent across all Sombrero samples ranging in temperature from 10 – 74 °C (**Figure 1**).
85 Minor differences are nevertheless visible (**Figure 2**); for example, *Thiomicrosrhabdus* and
86 *Sulfurospirillum* dominated Sombrero fluids with lower temperature, higher sulfate, and lower
87 sulfide. Warmer and more sulfidic Sombrero fluids included greater proportions of taxa that were
88 also abundant in fluids from Markers 3 and C (**Figure 2**).

89

90 **Markers 2 and 8**

91 The most sulfidic fluids were collected from chimneys near Marker 2 and Marker 8, which are
92 located on the western edge of the Lost City hydrothermal field (**Table 1; Figure 1;**
93 **Supplemental Figure S1**), and their microbial compositions were distinct from all other fluids.
94 One of the fluid samples from Marker 2 was dominated by a single ASV identical to the 16S
95 rRNA gene of *Alteromonas macleodi* (**Supplemental Table S2**), a ubiquitous marine bacterium
96 (5), suggesting substantial dilution of the sample with ambient seawater. Other samples from
97 Marker 2 also contained bacteria that have been previously associated with sulfur oxidation in
98 Lost City chimney biofilms, including the genera *Sulfurovum*, *Sulfurospirillum*, and
99 *Thiomicrosrhabdus* (3, 6, 7). Therefore, they are likely to be adapted to chimney habitats where
100 sulfidic hydrothermal fluids are mixing with oxic seawater, and they are probably not
101 representative of microbial communities inhabiting anoxic, subsurface environments. The
102 ribosomal RNA fraction of Marker 2 fluids contained elevated relative abundances of a
103 *Sulfurospirillum* ASV and a *Thiomicrosrhabdus* ASV (**Figure 2**). Microbial taxa detected in fluids

104 collected near Marker 8 were broadly similar to those of Marker 2 fluids, except that they were
105 dominated by one *Sulfurovum* ASV that was rare in Marker 2 fluids (**Figure 2**).
106

107 **Calypso**

108 The Calypso chimney sits on the eastern wall of the Atlantis Massif, approximately 75 m from
109 the large Poseidon edifice that dominates the Lost City field (**Figure 1**). The fluids venting from
110 Calypso had higher sulfide concentrations than the fluids from Markers 3 and C, but less sulfide
111 than in Markers 2 and 8 (**Table 1**). The overall microbial community structure resembled that of
112 Sombrero fluids (**Figure 1**), although the ASVs with the highest counts in Calypso were also
113 common in Markers 3 and C (**Figure 2**). The top *Thermodesulfovibrionia* ASV in Calypso fluids
114 differed by one base from the ASV that dominated the fluids from Markers C and 3. This ASV
115 was further enriched in the RNA fraction from Calypso, suggesting that it could have been
116 metabolically active prior to sampling.
117

118 ASVs classified as the ANME-1b group of archaeal methanotrophs were most abundant in fluids
119 from Calypso (**Figure 2**). ANME-1 sequences were rare or absent in almost all other fluid
120 samples except for a few samples from Markers C and 3 and the RNA (but not DNA) fraction
121 from one sample of fluids at Marker 2. These results are consistent with our previous studies
122 that documented very high relative abundances of ANME-1 in cooler chimneys at the periphery
123 of the field and trace levels of ANME-1 DNA in hot chimneys of the central Poseidon complex
124 (1, 3).

125
126 Calypso fluids were rich in Chloroflexi ASVs and metagenomic sequences primarily classified as
127 class *Dehalococcoidia* (**Supplemental Tables S2-S3**), but ASVs classified as *Anaerolineae*,
128 TK10, and KD4-96 were also present at low levels. The Chloroflexi MAG from Lost City biofilms

129 previously reported in (7) is a member of the *Anaerolineae*. *Dehalococcoidia* ASVs were
130 generally most abundant in Calypso fluids, but most ASVs were broadly distributed (**Figure 2**).
131
132

133
134 **DETAILED DESCRIPTIONS OF METAGENOME-ASSEMBLED GENOMES (MAGs)**

135 ***Methanosarcinaceae* MAG**

136 The predominant *Methanosarcinaceae* ASV was classified as genus *Methanosalsum* in the
137 SILVA database, but our phylogenies of 16S rRNA and mcrA indicate that the Lost City
138 *Methanosarcinaceae* are not monophyletic with any previously characterized genera
139 (**Supplemental Figure S5**). Over 254 bases, the *Methanosarcinaceae* ASV is 94% similar to
140 the 16S rRNA gene of *Methanococcoides methylutens* and 95.7% similar to that of
141 *Methanohalophilus mahii*.

142
143 The *Methanosarcinaceae* MAG contained 1276 coding sequences (CDS) and was estimated to
144 be 84% complete with 1% redundancy. It shares 99% average nucleotide identity (ANI) with the
145 MAG we previously recovered from a Lost City biofilm (7). It is most abundant in Marker 3 fluids
146 (**Figure 3**), and it is more abundant in those Sombrero fluids that show more mixing with
147 seawater (lower temperature, more sulfate, less sulfide), consistent with the distribution of
148 *Methanosarcinaceae* ASVs (**Figure 2**).

149
150 *Methanosarcinaceae* MAG-1276 has a remarkably low GC content (29%), which may help
151 explain why the first metagenomic studies of Lost City biofilms recovered surprisingly few
152 archaeal sequences (6, 8). It encodes the core pathway for methanogenesis from carbon
153 dioxide (**Supplemental Table S5**). It contains predicted sequences for F₄₂₀-reducing
154 hydrogenase (FrhAB), which is required by all methanogens that reduce carbon dioxide with H₂

155 (9). In addition, two genes predicted to encode subunits of Ech hydrogenase (EchCE) are
156 present. FrhB and EchCE are located on the same contig as a multicomponent Na⁺:H⁺
157 antiporter (MrpACBD) and the MAG's only gene annotated as a subunit of NADH-quinone
158 oxidoreductase (NuoH).

159

160 The MAG encodes AMP-forming acetyl-CoA synthetase, as previously reported for
161 *Methanosarcinaceae* in Lost City biofilms (7), which may enable acetoclastic methanogenesis. It
162 also encodes MtaA and MtaC (**Supplemental Table S5**), two of the three proteins that enable
163 the use of methanol as a substrate for methanogenesis in some methanogens.

164

165 *Methanosarcinaceae* MAG-1276 contains a complete 14-gene cluster (mbhA-N) encoding
166 membrane-bound hydrogenase (**Figure 5; Supplemental Figure S8**). The same gene cluster,
167 with conserved synteny, is also found in methanogens belonging to the order
168 *Methanomicrobiales* (e.g. *Methanospirillum hungatei*) and in heterotrophs of the order
169 *Thermococcales* (e.g. *Thermococcus kodakarensis*) (10). The mbhL subunits from these
170 methanogens have only 42-45% identities with the Lost City mbhL sequences reported here,
171 which have greater similarly (~49% identities) to mbhL sequences from *Thermococcus*.

172

173 As we reported previously for chimney biofilms (11), the *Methanosarcinaceae* MAG encodes a
174 formate dehydrogenase (FDH) that is similar to that of *Methanolobus* species, which are unable
175 to use formate as a carbon source. The contig encoding this FDH also encodes one subunit of
176 F₄₂₀-non-reducing hydrogenase (MvhD) and heterodisulfide reductase (HdrABC).

177

178 No known transporters for formate were identified in this MAG, but one gene was predicted to
179 encode a member of the oxalate:formate antiporter family. In *Oxalobacter formigenes*, this
180 transporter enables uptake of oxalate with export of formate (12). Its presence was also

181 observed in a formate-utilizing methanogen, which lacks any other formate transporters, in
182 hyperalkaline groundwaters of the Samail Ophiolite (13). Potentially homologous
183 oxalate:formate antiporters were also identified in two NPL-UPA2 MAGs and two
184 *Natronincolaceae* MAGs from Lost City fluids. The four bacterial sequences shared 59-63%
185 amino acid identities with the *Methanosarcinaceae* sequence.

186

187 ***Methanocellales* MAG**

188 A MAG classified as order *Methanocellales* (838 CDS; 84% complete with 1% redundancy) was
189 only present in Calypso fluids (**Figure 3**). Curiously, no ASVs were classified as
190 *Methanocellales*, and no previous studies have identified any methanogen taxa in Lost City
191 samples other than *Methanosarcinaceae*.

192

193 *Methanocellales* MAG-838 encodes the key enzyme CODH/ACS, but it has an incomplete
194 pathway for methanogenesis, including only four of the first five steps (FwdABCDEFG, Ftr, Mtd,
195 and Mer) and lacking all other steps, including the proteins required for methane production
196 (methyl-coenzyme M reductase and heterodisulfide reductase) (**Supplemental Table S5**).

197 Evidence for acetate utilization includes a predicted sequence for AMP-forming acetyl-CoA
198 synthetase, which shares 73% amino acid identities with the homolog in the
199 *Methanosarcinaceae* MAG, and a cation/acetate symporter (ActP). The MAG includes one
200 [NiFe] hydrogenase and the Rnf complex (RnfCDGEAB), an energy-conserving
201 ferredoxin:NAD⁺-oxidoreductase (14).

202

203 **ANME-1 MAG**

204 A MAG classified as ANME-1 (1099 CDS; 88% complete with 4% redundancy) was most
205 abundant in Calypso fluids as well as the Marker 2 metatranscriptome, even though ANME-1
206 was very rare in the Marker 2 metagenomes. As expected for ANME-1 archaea, the Lost City

207 ANME-1 MAG contains the core methanogenic pathway (**Supplemental Table S5**). The
208 absence of cytochromes and presence of hydrogenases in this MAG was noted by (15) as
209 consistent with the genomic features of the so-called “freshwater” clade of ANME-1, for which
210 the genus “Candidatus Methanoalium” was proposed. One of the shared features within this
211 clade, including the Lost City ANME-1 MAG, is a novel HdrABC-MvhADG complex (15), which
212 is involved in the transfer of electrons derived from H₂ in methanogens.

213

214 The Lost City ANME-1 MAG contains the core methanogenic pathway (**Supplemental Table**
215 **S5**), including F₄₂₀-dependent methylenetetrahydromethanopterin reductase (Mer). This gene is
216 required for methanogenesis from carbon dioxide, but it is typically absent in ANME genomes,
217 with at least one exception previously reported (16). The MAG lacks all but one of the subunits
218 of N⁵-methyl-H₄MPT:coenzyme M methyltransferase (Mtr), which catalyzes the penultimate step
219 of methanogenesis (and putatively the second step of reverse methanogenesis). It is present in
220 most but not all ANME-1 genomes (15).

221

222 The ANME-1 MAG-1 also encodes the complete mbhA-N gene cluster for membrane-bound
223 hydrogenase (**Figure 5; Supplemental Figure S8**), and each predicted gene in the cluster has
224 the greatest similarity to the homolog in the *Methanosarcinaceae* MAG than to any other
225 sequences in public databases. It lacks any established genes for FDH, but it includes a
226 divergent FDH-like sequence that appears to be homologous to those found in other Lost City
227 MAGs (**Figure 6; Supplemental Figure S9**). Distant homologs of FDH have been previously
228 identified in ANME genomes, but they do not share significant sequence similarity with the FDH-
229 like sequences reported here.

230

231 **Bipolariaulota MAGs**

232 ASVs classified as Bipolaricaulota (named Acetothermia in the SILVA database) clustered into
233 three distinct clades (**Supplemental Figure S6**) that correspond to the taxonomic classifications
234 of three distinct Bipolaricaulota MAGs. The most abundant of the three Bipolaricaulota MAGs
235 (1207 CDS; 86% complete with 0% redundancy) was classified by GTDB as species UBA7950
236 within class Bipolaricaulia, and it shares 99% ANI with the GTDB reference genome, which was
237 assembled by (17) with sequences from a previously published Lost City biofilm metagenome
238 (11). Bipolaricaulota MAG-1207 is most abundant in Sombrero and Calypso, especially the
239 Sombrero metatranscriptome (**Figure 3**). It encodes a nearly complete glycolysis pathway, an
240 incomplete TCA cycle, an incomplete Wood-Ljungdahl pathway, the Rnf complex, and pyruvate
241 formate-lyase (PflD) (**Supplemental Table S5**). The key enzyme of the Wood-Ljungdahl
242 pathway, CODH/ACS, is represented by the subunits AcsABC, although at least one subunit
243 (AcsB) appears to be replaced by the archaeal form (CdhC), according to GhostKoala results. A
244 thorough phylogenetic analysis of CODH/ACS subunits in Lost City MAGs is outside the scope
245 of the present study, but this initial observation is consistent with observations in MAGs from
246 other serpentinization-associated environments (18).

247
248 A second Bipolaricaulota MAG (1260 CDS; 89% complete with 1% redundancy) was classified
249 as family UBA9294 within order UBA7950, and it shares only 77% ANI with the closest
250 reference in GTDB (**Supplemental Table S4**). Bipolaricaulota MAG-1260 has a similar
251 complement of genes as in MAG-1207, including an incomplete Wood-Ljungdahl pathway
252 (CODH/ACS subunits AcsBC and CooC) and the Rnf complex, though it lacks pyruvate
253 formate-lyase and glycine reductase.

254
255 Neither of these Bipolaricaulota MAGs contains any known hydrogenases or formate
256 dehydrogenases. A divergent FDH-like sequence that appears to be homologous with those in
257 the *Methanosarcinaceae*, ANME-1, and *Thermodesulfovibrionales* MAGs was observed in

258 multiple initial BinSanity bins classified as Bipolaricaulota (**Figure 6**, but it was not included in
259 the three re-assembled, refined Bipolaricaulota MAGs. The most similar sequence in the NCBI
260 NR database was from a MAG assembled by (17) from a Voltri Massif serpentinite spring (19).
261
262 A third Bipolaricaulota MAG (1503 CDS; 92% complete with 1% redundancy) was classified as
263 genus UBA3574 within family Bipolaricaulaceae. It encodes a nearly complete Wood-Ljungdahl
264 pathway (including CODH/ACS subunits AcsBCDE and CooC) and the NADP-dependent
265 formate dehydrogenase (FdhA) that is typical of acetogens. It does not encode the Rnf complex,
266 but it contains genes encoding all subunits of the heterodisulfide reductase complex MvhAGD-
267 HdrABC. It encodes a [NiFe] hydrogenase (HoxYH) and at least a partial gene cluster for
268 membrane-bound hydrogenase, including the large catalytic subunit MbhL (**Figure 5**;
269 **Supplemental Figure S8**). The predicted MbhL sequence is most closely related to two
270 Bipolaricaulota MAGs from hydrothermal systems: the Mid-Cayman Rise (20) and Guaymas
271 Basin (21). Bipolaricaulota MAG-1503 also encodes an oxalate:formate antiporter distinct from
272 those found in the *Methanosaerincinaceae*, NPL-UPA2, and *Natriniincolaceae* MAGs (31-33%
273 amino acid identities).

274

275 ***Thermodesulfovibrionales* MAG**

276 Two ASVs classified as *Thermodesulfovibrionia* (a class within phylum Nitrospirae) differed from
277 each other by a single base. One of these was the top ASV in each of the fluid samples from
278 Markers 3 and C (8-24% of all sequences), while the second ASV dominated the Calypso fluids
279 (7-17% of all DNA fractions and 27% of the RNA fraction). Lost City *Thermodesulfovibrionia*
280 metagenomic sequences and ASVs were notably rare in the low-sulfide fluids from Camel
281 Humps and the high-sulfide fluids from Marker 2 (**Figures 2-3**).
282

283 Accordingly, a MAG (1293 CDS; 92% complete with 0% redundancy) classified as order
284 *Thermodesulfovibrionales* within class *Thermodesulfovibrionia* was most abundant in Marker 3
285 and Calypso fluids. For heterotrophic metabolism, it encodes a nearly complete glycolysis
286 pathway and TCA cycle, plus genes for lactate dehydrogenase, pyruvate ferredoxin
287 oxidoreductase (PorABCD), and an oxalate:formate antiporter distinct from those found in the
288 *Methanosarcinaceae*, NPL-UPA2, and *Natrinicolaceae* MAGs (21-24% amino acid identities),
289

290 *Thermodesulfovibrionales* MAG-1293 has a partial Wood-Ljungdahl pathway and a monomeric
291 CO dehydrogenase (CooS) with two maturation factors (CooF and CooC). It encodes the
292 NAD(P)-dependent formate dehydrogenase typical of acetogens (FdhA), as well as aerobic
293 formate dehydrogenase (FdoG) and the divergent FDH-like sequence also observed in other
294 Lost City MAGs (**Figure 6**). It encodes a [NiFe]-hydrogenase (HyaAB) classified as [NiFe]
295 Group 1c, a group of respiratory H₂-uptake hydrogenases that can use fumarate, sulfate, or
296 metals as terminal electron acceptors. The MAG contains only one subunit of membrane-bound
297 hydrogenase (MbhJ), which shares 43-49% amino acid identities with the MbhJ sequences of
298 the other Lost City MAGs shown in **Figure 5**. The key genes required for nitrogen fixation
299 (nifHDK) and dissimilatory sulfate reduction (dsrAB) are present.

300

301 **Desulfotomaculum MAGs**

302 Two MAGs classified as family *Desulfotomaculaceae* were resolved based on their distinct
303 coverage patterns. Both MAGs were estimated to be 94% complete with 0% redundancy, but
304 one had more predicted genes (1580) than the other (1144). *Desulfotomaculaceae* MAG-1580
305 was only abundant in one sample from Sombrero, while MAG-1144 was abundant in Marker 3,
306 Sombrero, and Calypso fluids (**Figure 3**). Several ASVs were classified as genus
307 *Desulfotomaculum* within the family *Desulfotomaculaceae*. One of these was most abundant in
308 Marker 3 (up to 14% of all sequences) and Calypso (2-8% of all sequences), roughly matching

309 the distribution of MAG-1144, while another ASV (differing from the first by four bases) was only
310 abundant in Sombrero fluids, similar to MAG-1580 (**Figure 2**).

311

312 Both *Desulfotomaculum* MAGs encode a complete or nearly complete glycolysis pathway and at
313 least two genes of the TCA cycle (malate dehydrogenase and isocitrate dehydrogenase). In
314 addition, *Desulfotomaculum* MAG-1144 has succinate dehydrogenase (SdhABC) and the beta
315 subunit of fumarate dehydratase. *Desulfotomaculum* MAG-1580 encodes pyruvate ferredoxin
316 oxidoreductase (PorABCD) and pyruvate formate-lyase (PflD). Both MAGs have a
317 cation/acetate symporter (ActP), and MAG-1580 encodes a phosphonate transporter (PhnCDE).

318

319 Both MAGs have incomplete Wood-Ljungdahl pathways that lack the key enzyme CODH/ACS.
320 Both MAGs also have monomeric CO dehydrogenase (CooS) and aerobic formate
321 dehydrogenase (FdoG). No [NiFe] hydrogenases were detected, and only one subunit of [FeFe]
322 hydrogenase (HndC) was present in the *Desulfotomaculum* MAGs. This hydrogenase is
323 capable of H₂ oxidation with reduction of NADP in some organisms (22), but the presence of
324 only one subunit in multiple Lost City MAGs (**Supplemental Table S5**) is curious and has
325 unknown implications for the ability of these organisms to metabolize H₂.

326

327 The two *Desulfotomaculum* MAGs, in addition to the *Thermodesulfovibionales* MAG, are the
328 only MAGs reported here that encode dissimilatory sulfite reductase (DsrAB).

329 *Desulfotomaculum* dsrAB sequences were most abundant in Sombrero fluids, while
330 *Thermodesulfovibionales* dsrAB sequences were most abundant in Marker 3 and Calypso
331 fluids. The two *Desulfotomaculum* MAGs also have the key genes required for nitrogen fixation
332 (nifHDK).

333

334 **Natronincolaceae MAGs**

335 Two MAGs were classified as family *Natronincolaceae* within the Clostridia and shared 81-89%
336 ANI with a MAG reconstructed from seafloor borehole fluids at North Pond (23). Other genera
337 within the family *Natronincolaceae* include *Alkaliphilus* and *Serpentinicella*, which have been
338 isolated from the Prony Bay hydrothermal field (24, 25). The coverage of the *Natronincolaceae*
339 MAGs was primarily in Sombrero fluids. The two MAGs shared 80% ANI but showed a few
340 potentially important differences in their genomic inventories.

341

342 *Natronincolaceae* MAG-2163 (2163 CDS; 90% complete with 3% redundancy) has one of the
343 largest genomes in this study, and it has an incomplete glycolysis pathway and incomplete TCA
344 cycle. It encodes at least three steps of the Wood-Ljungdahl pathway, monomeric CODH
345 (CooS), the Rnf complex, and the electron carriers HdrABC and MvhD.

346

347 In contrast, *Natronincolaceae* MAG-1138 (1138 CDS; 75% complete with 0% redundancy) has
348 a smaller genome, a nearly complete glycolysis pathway, and no TCA cycle. It includes two
349 genes associated with the Wood-Ljungdahl pathway, but not CODH, Rnf, Hdr, or MvhD. It does
350 include acetate kinase (AckA) and phosphotransacetylase (Pta). It lacks any genes for ATP
351 synthase, suggesting an obligate fermentative lifestyle.

352

353 *Natronincolaceae* MAG-2163 has [FeFe] hydrogenase (HndBCD), while MAG-1138 only has the
354 HndC subunit. Both *Natronincolaceae* MAGs have at least one subunit of pyruvate
355 dehydrogenase and pyruvate ferredoxin oxidoreductase, though they differ in which subunits
356 they include (**Supplemental Table S5**).

357

358 ***Dehalococcoidia* MAGs**

359 The most abundant *Dehalococcoidia* MAG (844 CDS; 73% complete with 0% redundancy) was
360 classified as family SpSt-899 within order SZUA-161. It was one of the highest coverage MAGs

361 in Calypso fluids as well as the Sombrero and Marker 2 metatranscriptomes. Unlike the other
362 two *Dehalococcoidia* MAGs described below, glycolysis and the TCA cycle are incomplete, and
363 there are no genes required for the degradation of large organic compounds. However, the
364 presence of pyruvate:ferredoxin oxidoreductase, pyruvate formate-lyase, and an
365 oxalate/formate antiporter suggest the ability to ferment low-molecular-weight organic
366 compounds. In addition, the MAG has two steps of the Wood-Ljungdahl pathway (FchA and
367 MetF), the Rnf complex, and a complete set of genes encoding the key enzyme CODH/ACS. No
368 hydrogenases or formate dehydrogenases are present. Curiously, *Dehalococcoidia* MAG-844
369 has V(A)-type ATP synthase, which is typically associated with archaea, but has also been
370 observed in Chloroflexi and Parcubacteria in another serpentinite-hosted spring (26).

371

372 Two additional *Dehalococcoidia* MAGs belong to the SAR202 cluster, one of which was
373 classified by GTDB as order SAR202 and one as order UBA3495. Each MAG has 98% ANI with
374 previously published marine Chloroflexi MAGs (**Supplemental Table S4**). *Dehalococcoidia*
375 MAG-2669 (2669 CDS; 86% complete with 4% redundancy) has moderately high coverage in
376 all chimney fluids except for Marker 3. *Dehalococcoidia* MAG-2875 (2875 CDS; 87% complete
377 with 1% redundancy) was less abundant than MAG-2669 in all samples but otherwise exhibited
378 a similar distribution pattern. Both MAGs encoded nearly complete glycolysis pathways and
379 TCA cycles, and they have a variety of genes associated with the oxidation of various organic
380 molecules, consistent with previous studies of marine Chloroflexi (27, 28). Both MAGs encode
381 cytochrome c oxidase (CoxA), which represents the only evidence for aerobic respiration in any
382 of the final, refined MAGs. *Dehalococcoidia* MAG-2875 has both (aerobic) pyruvate
383 dehydrogenase and (anaerobic) pyruvate:ferredoxin oxidoreductase, as reported for other
384 SAR202 genomes (29), while MAG-2669 has neither. Neither MAG encodes any FDH or
385 hydrogenases. MAG-2669 is predicted to encode sulfite reductase (Sir), adenylylsulfate
386 reductase (AprAB), and sulfate adenylyltransferase (Sat), but dissimilatory sulfite reductase

387 (DsrAB) is not present. Both MAGs have genes associated with the metabolism of organosulfur
388 compounds, similar to those reported by (29) for deep-sea SAR202 genomes (**Supplemental**
389 **Table S5**).

390

391 All three *Dehalococcoidia* MAGs include genes for glycine reductase, thioredoxin, and
392 selenocysteine synthesis. GrdB (beta subunit of glycine reductase) sequences from the two
393 Lost City Dehalococcoidia MAGs that belong to the SAR202 marine cluster (MAG-2669 and
394 MAG-2875) are distinct from the GrdB of *Dehalococcoidia* MAG-844 and from the GrdB of all
395 other Lost City MAGs (**Supplemental Figure S11**).

396

397 **NPL-UPA2 MAGs**

398 Three MAGs classified as candidate phylum NPL-UPA2 (new name *Candidatus Horikoshi*
399 bacteria proposed by (30) were recovered, each only 55-72% complete and with distinct
400 coverage patterns among the hydrothermal fluid samples. No ASVs or unclassified reads were
401 classified as NPL-UPA2, as this group was not yet represented in the SILVA or Kaiju databases.
402 NPL-UPA2 MAG-914 (914 CDS; 62% complete with 0% redundancy) and MAG-1083 (1083
403 CDS; 55% complete with 3% redundancy) were most abundant in Calypso fluids and nearly
404 absent in all other locations. MAG-718 (718 CDS; 72% complete with 3% redundancy) was
405 most abundant in Marker 3 fluids and exhibited a nearly inverse abundance distribution
406 compared to the other two MAGs. All three NPL-UPA2 MAGs have incomplete Wood-Ljungdahl
407 pathways that lack the first few steps and begin with methylene-THF dehydrogenase (Fold),
408 and all three MAGs encode V(A)-type ATP synthase and the Rnf complex, as reported by (30).

409

410 In most other respects the two NPL-UPA2 MAGs that are prominent in Calypso fluids differ from
411 the MAG that is most abundant in Marker 3 fluids. The Calypso MAGs encode multiple subunits
412 of the CODH/ACS enzyme, while MAG-718 has only the methyltransferase subunit (AcsE).

413 MAG-1083 also includes acetate kinase (AckA), phosphotransacetylase (Pta), and a
414 cation/acetate symporter (ActP). In contrast, MAG-718 is the only NPL-UPA2 MAG that
415 encodes pyruvate formate-lyase (PflD), the oxalate/formate antiporter, and carbonic anhydrase.

416

417 Evidence for hydrogenases in the NPL-UPA2 MAGs is lacking. Membrane-bound hydrogenase
418 (MbhL) was identified in two of the MAGs by GhostKoala, but Prokka annotated these
419 sequences as NAD(P)H-quinone oxidoreductase and formate hydrogenlyase. Neither sequence
420 could be placed in the mbhL phylogeny of **Figure 5**. MAG-1083 includes one subunit of F₄₂₀-
421 reducing hydrogenase (FrhB) and one subunit of [FeFe] hydrogenase (HndD), but the functional
422 roles of these predicted proteins are unclear.

423

424 Unlike the NPL-UPA2 MAG reported by (30), none of the Lost City NPL-UPA2 MAGs have
425 formate dehydrogenase nor the electron carriers Hdr and Etf.

426

427 **Patescibacteria MAGs**

428 Several MAGs classified as candidate phylum Patescibacteria were represented by two classes:
429 Paceibacteria and Gracilibacteria (according to GTDB taxonomy). Paceibacteria MAGs (55-86%
430 completion with 0-3% redundancy) had small genomes (as low as 307 kb with 63% estimated
431 completion) with low GC content (24-45%). Gracilibacteria MAGs (61-83% completion with 0-
432 1% redundancy) had even lower GC content (22-34%) and somewhat larger genomes but with
433 very low annotation success. As few as 8% of all coding sequences in Gracilibacteria MAGs
434 yielded GhostKoala results. Two of the Paceibacteria MAGs were most abundant in Marker 3
435 fluids, while Gracilibacteria MAGs were notably absent in Marker 3 fluids and were more
436 abundant in Camel Humps and Sombrero fluids (**Figure 3; Supplemental Table S4**).

437

438 In general, Paceibacteria and Gracilibacteria MAGs included genes for the biosynthesis of key
439 cellular components and basic information processing, but genes specific to catabolic pathways
440 were rare. The few exceptions included a lactate transporter (LctP) that was present in the two
441 highest-coverage Paceibacteria MAGs, and one of these MAGs also has lactate dehydrogenase
442 (LdhA). In addition, acetate kinase (AckA), acylphosphatase (AcyP), and phosphoenolpyruvate
443 synthase (PpsA) were present in one or more Paceibacteria MAGs (**Supplemental Table S5**).
444 Propionyl-CoA carboxylase (PccB) was included in one Gracilibacteria MAG. All Paceibacteria
445 MAGs, one of the Gracilibacteria MAGs, and almost all other MAGs in this study have a
446 substrate-binding protein associated with the peptide/nickel transport system (K02035;
447 **Supplemental Table S6**).

448
449 Curiously, methylene tetrahydrofolate dehydrogenase (Fold), which is part of the Wood-
450 Ljungdahl pathway, was encoded by three Paceibacteria MAGs and one Gracilibacteria MAG.
451 Fold was also observed in 17 MAGs from The Cedars, a serpentinite-hosted spring in
452 California, that were classified as candidate phylum OD1 (26), now included within
453 Paceibacteria in GTDB.

454
455 As mentioned in the main text, ATP synthase was completely absent in three of the
456 Paceibacteria MAGs, and one Gracilibacteria MAG included only a single subunit. One
457 Paceibacteria MAG encodes a V(A)-type ATP synthase instead of the F-type ATP synthase
458 present in the other Paceibacteria and Gracilibacteria MAGs. MAGs that were classified as
459 candidate phylum OD1 from The Cedars also encoded V(A)-type ATP synthase or lacked any
460 ATP synthase at all (26).

461

462 **WOR-3 MAG**

463 One of the highest-coverage MAGs in Marker 3 and Sombrero fluids was classified as
464 candidate phylum WOR-3, which was previously identified in methane-rich marine sediments
465 (31) and was proposed to be renamed as *Candidatus Stahlbacteria* (32). The WOR-3 MAG
466 (59% completion with 0% redundancy) has a partial glycolysis pathway, perhaps explainable by
467 the incompleteness of the MAG, and no TCA cycle. Other genes possibly indicative of organic
468 carbon catabolism include those predicted to encode one subunit of pyruvate dehydrogenase
469 (PdhD), pyruvate formate-lyase (PflD), formate dehydrogenase (FdoG), and a cation/acetate
470 symporter (ActP). Like the NPL-UPA2 MAGs, one Paceibacteria MAG, and the archaeal MAGs,
471 the WOR-3 MAG encodes a V(A)-type ATP synthase.

472

473 The WOR-3 formate dehydrogenase shares a maximum of only ~31% amino acid identities with
474 any other sequences in the NCBI NR and JGI IMG “all isolates” databases. This divergent FDH-
475 like sequence in the WOR-3 MAG is distinct from the divergent FDH-like sequence described
476 above for other Lost City MAGs (**Figure 6**), and in both cases, additional research is required to
477 establish whether their functions are indeed associated with formate metabolism.

478

479 **References**

- 480 1. Brazelton WJ, Schrenk MO, Kelley DS, Baross JA. 2006. Methane- and Sulfur-
481 Metabolizing Microbial Communities Dominate the Lost City Hydrothermal Field
482 Ecosystem. *Appl Environ Microbiol* 72:6257–6270.
- 483 2. Schrenk MO, Kelley DS, Bolton SA, Baross JA. 2004. Low archaeal diversity linked to
484 subseafloor geochemical processes at the Lost City Hydrothermal Field, Mid-Atlantic
485 Ridge. *Environ Microbiol* 6:1086–1095.
- 486 3. Brazelton WJ, Ludwig KA, Sogin ML, Andreishcheva EN, Kelley DS, Shen C-C, Edwards
487 RL, Baross JA. 2010. Archaea and bacteria with surprising microdiversity show shifts in

- 488 dominance over 1,000-year time scales in hydrothermal chimneys. Proceedings of the
489 National Academy of Sciences 107:1612–1617.
- 490 4. Brazelton WJ, Mehta MP, Kelley DS, Baross JA. 2011. Physiological Differentiation within
491 a Single-Species Biofilm Fueled by Serpentinization. *mBio* 2:e00127-11.
- 492 5. Koch H, Germscheid N, Freese HM, Noriega-Ortega B, Lücking D, Berger M, Qiu G,
493 Marzinelli EM, Campbell AH, Steinberg PD, Overmann J, Dittmar T, Simon M, Wietz M.
494 2020. Genomic, metabolic and phenotypic variability shapes ecological differentiation and
495 intraspecies interactions of *Alteromonas macleodii*. *Sci Rep* 10:809.
- 496 6. Brazelton WJ, Baross JA. 2010. Metagenomic Comparison of Two *Thiomicrospira*
497 Lineages Inhabiting Contrasting Deep-Sea Hydrothermal Environments. *PLoS ONE*
498 5:e13530.
- 499 7. McGonigle JM, Lang SQ, Brazelton WJ. 2020. Genomic Evidence for Formate Metabolism
500 by *Chloroflexi* as the Key to Unlocking Deep Carbon in Lost City Microbial Ecosystems.
501 *Appl Environ Microbiol* 86:e02583-19.
- 502 8. Brazelton WJ, Baross JA. 2009. Abundant transposases encoded by the metagenome of a
503 hydrothermal chimney biofilm. *ISME J* 3:1420–1424.
- 504 9. Mand TD, Metcalf WW. 2019. Energy Conservation and Hydrogenase Function in
505 Methanogenic Archaea, in Particular the Genus *Methanosarcina*. *Microbiol Mol Biol Rev*
506 83.
- 507 10. Thauer RK, Kaster A-K, Goenrich M, Schick M, Hiromoto T, Shima S. 2010. Hydrogenases
508 from Methanogenic Archaea, Nickel, a Novel Cofactor, and H₂ Storage. *Annu Rev*
509 *Biochem* 79:507–536.

- 510 11. Lang SQ, Früh-Green GL, Bernasconi SM, Brazelton WJ, Schrenk MO, McGonigle JM.
511 2018. Deeply-sourced formate fuels sulfate reducers but not methanogens at Lost City
512 hydrothermal field. *Sci Rep* 8:755.
- 513 12. Abe K, Ruan Z-S, Maloney PC. 1996. Cloning, Sequencing, and Expression in *Escherichia*
514 *coli* of OxIT, the Oxalate:Formate Exchange Protein of *Oxalobacter formigenes*(*). *Journal*
515 *of Biological Chemistry* 271:6789–6793.
- 516 13. Fones EM, Colman DR, Kraus EA, Stepanauskas R, Templeton AS, Spear JR, Boyd ES.
517 2021. Diversification of methanogens into hyperalkaline serpentizing environments
518 through adaptations to minimize oxidant limitation. *ISME J* 15:1121–1135.
- 519 14. Biegel E, Schmidt S, González JM, Müller V. 2011. Biochemistry, evolution and
520 physiological function of the Rnf complex, a novel ion-motive electron transport complex in
521 prokaryotes. *Cell Mol Life Sci* 68:613–634.
- 522 15. Chadwick GL, Skennerton CT, Laso-Pérez R, Leu AO, Speth DR, Yu H, Morgan-Lang C,
523 Hatzenpichler R, Goudeau D, Malmstrom R, Brazelton WJ, Woyke T, Hallam SJ, Tyson
524 GW, Wegener G, Boetius A, Orphan VJ. 2022. Comparative genomics reveals electron
525 transfer and syntrophic mechanisms differentiating methanotrophic and methanogenic
526 archaea. *PLOS Biology* 20:e3001508.
- 527 16. Beulig F, Røy H, McGlynn SE, Jørgensen BB. 2019. Cryptic CH₄ cycling in the sulfate–
528 methane transition of marine sediments apparently mediated by ANME-1 archaea. *ISME J*
529 13:250–262.
- 530 17. Parks DH, Chuvochina M, Rinke C, Mussig AJ, Chaumeil P-A, Hugenholtz P. 2021. GTDB:
531 an ongoing census of bacterial and archaeal diversity through a phylogenetically

- 532 consistent, rank normalized and complete genome-based taxonomy. Nucleic Acids Res
533 <https://doi.org/10.1093/nar/gkab776>.
- 534 18. Nobu MK, Nakai R, Tamazawa S, Mori H, Toyoda A, Ijiri A, Suzuki S, Kurokawa K,
535 Kamagata Y, Tamaki H. 2021. Unique metabolic strategies in Hadean analogues reveal
536 hints for primordial physiology.
- 537 19. Brazelton WJ, Thornton CN, Hyer A, Twing KI, Longino AA, Lang SQ, Lilley MD, Fröh-
538 Green GL, Schrenk MO. 2017. Metagenomic identification of active methanogens and
539 methanotrophs in serpentinite springs of the Voltri Massif, Italy. PeerJ 5:e2945.
- 540 20. Zhou Z, Liu Y, Pan J, Cron BR, Toner BM, Anantharaman K, Breier JA, Dick GJ, Li M.
541 2020. Gammaproteobacteria mediating utilization of methyl-, sulfur- and petroleum organic
542 compounds in deep ocean hydrothermal plumes. ISME J 14:3136–3148.
- 543 21. Dombrowski N, Teske AP, Baker BJ. 2018. Expansive microbial metabolic versatility and
544 biodiversity in dynamic Guaymas Basin hydrothermal sediments. Nat Commun 9:4999.
- 545 22. Kpebe A, Benvenuti M, Guendon C, Rebai A, Fernandez V, Le Laz S, Etienne E,
546 Guigliarelli B, García-Molina G, de Lacey AL, Baffert C, Brugna M. 2018. A new
547 mechanistic model for an O₂-protected electron-bifurcating hydrogenase, Hnd from
548 *Desulfovibrio fructosovorans*. Biochimica et Biophysica Acta (BBA) - Bioenergetics
549 1859:1302–1312.
- 550 23. Tully BJ, Wheat CG, Glazer BT, Huber JA. 2018. A dynamic microbial community with high
551 functional redundancy inhabits the cold, oxic subseafloor aquifer. ISME J 12:1–16.
- 552 24. Mei N, Postec A, Erauso G, Joseph M, Pelletier B, Payri C, Ollivier B, Quéméneur M.
553 2016. *Serpentinicella alkaliphila* gen. nov., sp. nov., a novel alkaliphilic anaerobic

- 554 bacterium isolated from the serpentinite-hosted Prony hydrothermal field, New Caledonia.
- 555 Int J Syst Evol Microbiol 66:4464–4470.
- 556 25. Postec A, Quéméneur M, Lecoeuvre A, Chabert N, Joseph M, Erauso G. 2021. Alkaliphilus
557 serpentinus sp. nov. and Alkaliphilus pronyensis sp. nov., two novel anaerobic alkaliphilic
558 species isolated from the serpentinite-hosted Prony Bay Hydrothermal Field (New
559 Caledonia). Systematic and Applied Microbiology 44:126175.
- 560 26. Suzuki S, Ishii S, Hoshino T, Rietze A, Tenney A, Morrill PL, Inagaki F, Kuenen JG,
561 Nealson KH. 2017. Unusual metabolic diversity of hyperalkaliphilic microbial communities
562 associated with subterranean serpentinization at The Cedars. ISME J 11:2584–2598.
- 563 27. Liu R, Wei X, Wang L, Cao J, Song W, Wu J, Thomas T, Jin T, Wang Z, Wei W, Wei Y,
564 Zhai H, Yao C, Shen Z, Fang J. 2021. Novel Chloroflexi Genomes From The Deepest
565 Ocean Reveal Metabolic Strategies For The Adaptation To Deep-Sea Habitats
566 <https://doi.org/10.21203/rs.3.rs-254541/v2>.
- 567 28. Landry Z, Swan BK, Herndl GJ, Stepanauskas R, Giovannoni SJ. SAR202 Genomes from
568 the Dark Ocean Predict Pathways for the Oxidation of Recalcitrant Dissolved Organic
569 Matter. mBio 8:e00413-17.
- 570 29. Mehrshad M, Rodriguez-Valera F, Amoozegar MA, López-García P, Ghai R. 2018. The
571 enigmatic SAR202 cluster up close: shedding light on a globally distributed dark ocean
572 lineage involved in sulfur cycling. ISME J 12:655–668.
- 573 30. Suzuki S, Nealson KH, Ishii S. 2018. Genomic and in-situ Transcriptomic Characterization
574 of the Candidate Phylum NPL-UPL2 From Highly Alkaline Highly Reducing Serpentinized
575 Groundwater. Frontiers in Microbiology 9:3141.

576 31. Baker BJ, Lazar CS, Teske AP, Dick GJ. 2015. Genomic resolution of linkages in carbon,
577 nitrogen, and sulfur cycling among widespread estuary sediment bacteria. *Microbiome*
578 3:14.

579 32. Dombrowski N, Seitz KW, Teske AP, Baker BJ. 2017. Genomic insights into potential
580 interdependencies in microbial hydrocarbon and nutrient cycling in hydrothermal
581 sediments. *Microbiome* 5:106.

582

Tables and Figures

Brazelton et al. “Metabolic strategies shared by basement residents of the Lost City hydrothermal field”

Tables

1. Sample overview including temp and chemistry

Figures

1. Map and ordination
2. 16S bubbles
3. MAG bubbles
4. MAG presence/absence of key genes
5. MBH phylogeny
6. FDH phylogeny
7. Key gene bubbles

Supplemental Figures

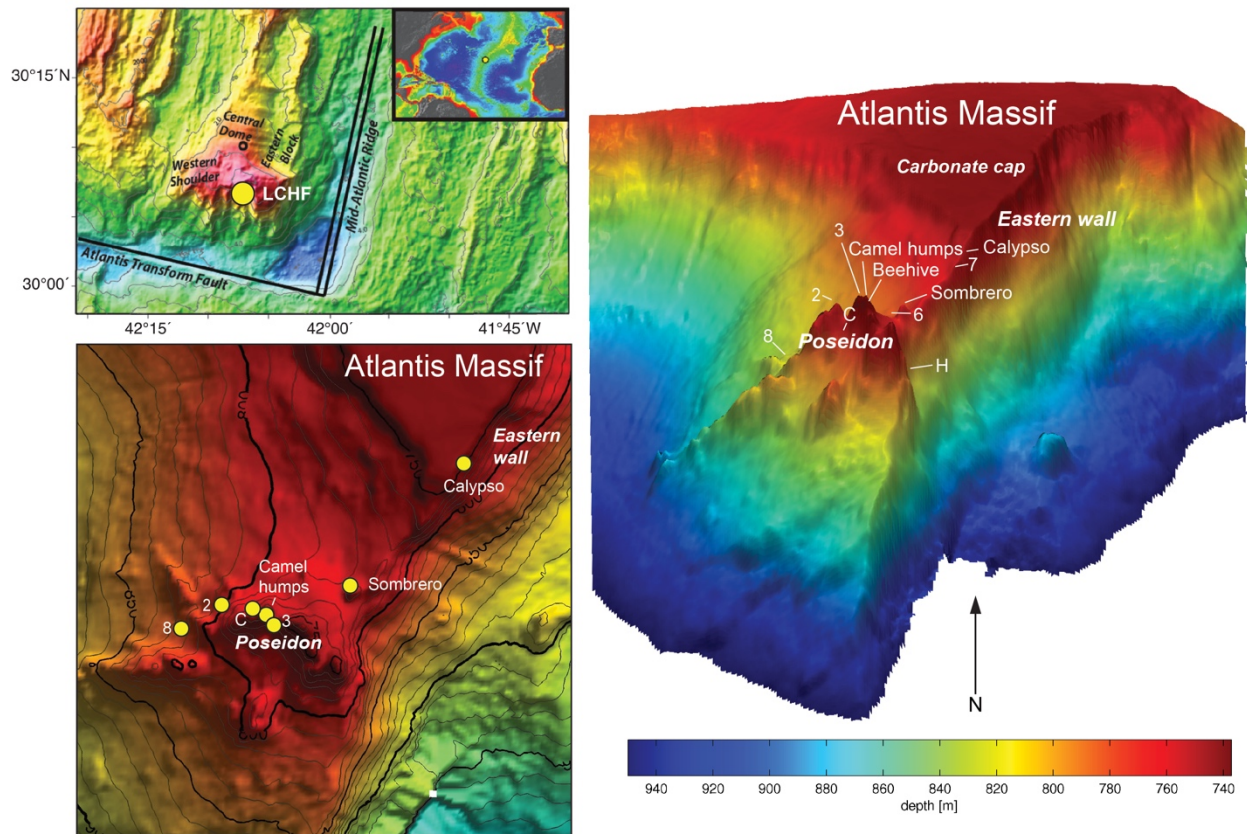
1. Extended map figure
2. Chimney photos
3. Metagenome analysis workflow
4. Kaiju bubbles
5. Phylogeny – Methanosaericales 16S + mcrA
6. Phylogeny – Bipolaricauota 16S
7. Phylogeny – Thermodesulfovibrionales 16S
8. Phylogeny + gene order mbhL
9. Phylogeny + gene order FDH
10. Phylogeny – carbonic anhydrase
11. Phylogeny – GrdB
12. Hydrogenase bubbles
13. Acetate/formate bubbles
14. Methanogenesis bubbles
15. Acetogenesis bubbles

Supplemental Tables (Excel files)

1. Sample info
2. Full 16S count table including contaminants
3. Kaiju tables
4. MAG taxonomy, completeness, coverage table
5. MAG gene presence absence tables
6. MAG annotations for transporters, dbCAN, FeGenie
7. KO coverage table
8. Incubation experiment results

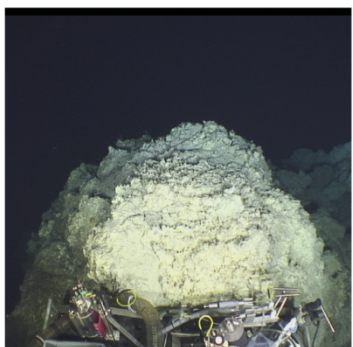
Github Repo

1. Protocols
2. Kaiju Krona plots
3. NCBI SRA and GenBank metadata
4. MAG sequences and annotations
5. Alignments and sequences for phylogenetic trees
6. R code for plots
7. Python scripts for metagenomic analyses

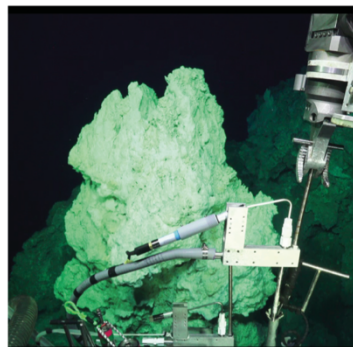


Supplemental Figure S1. Extended version of **Figure 1** showing the location of the Lost City hydrothermal field near the summit of the Atlantis Massif, which is located northwest of the intersection of the Mid-Atlantic Ridge and the Atlantis Transform Fault.

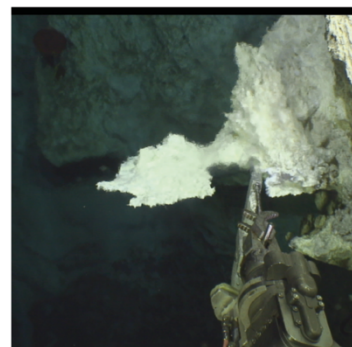
Camel Humps



Marker 3



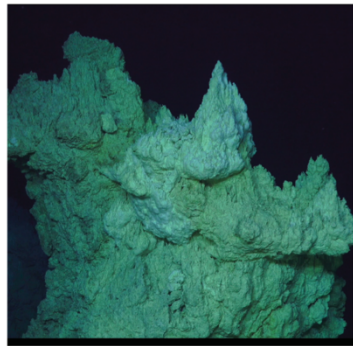
Marker 2



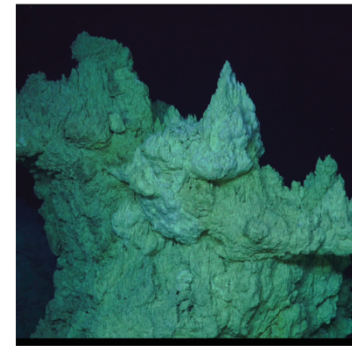
Calypso



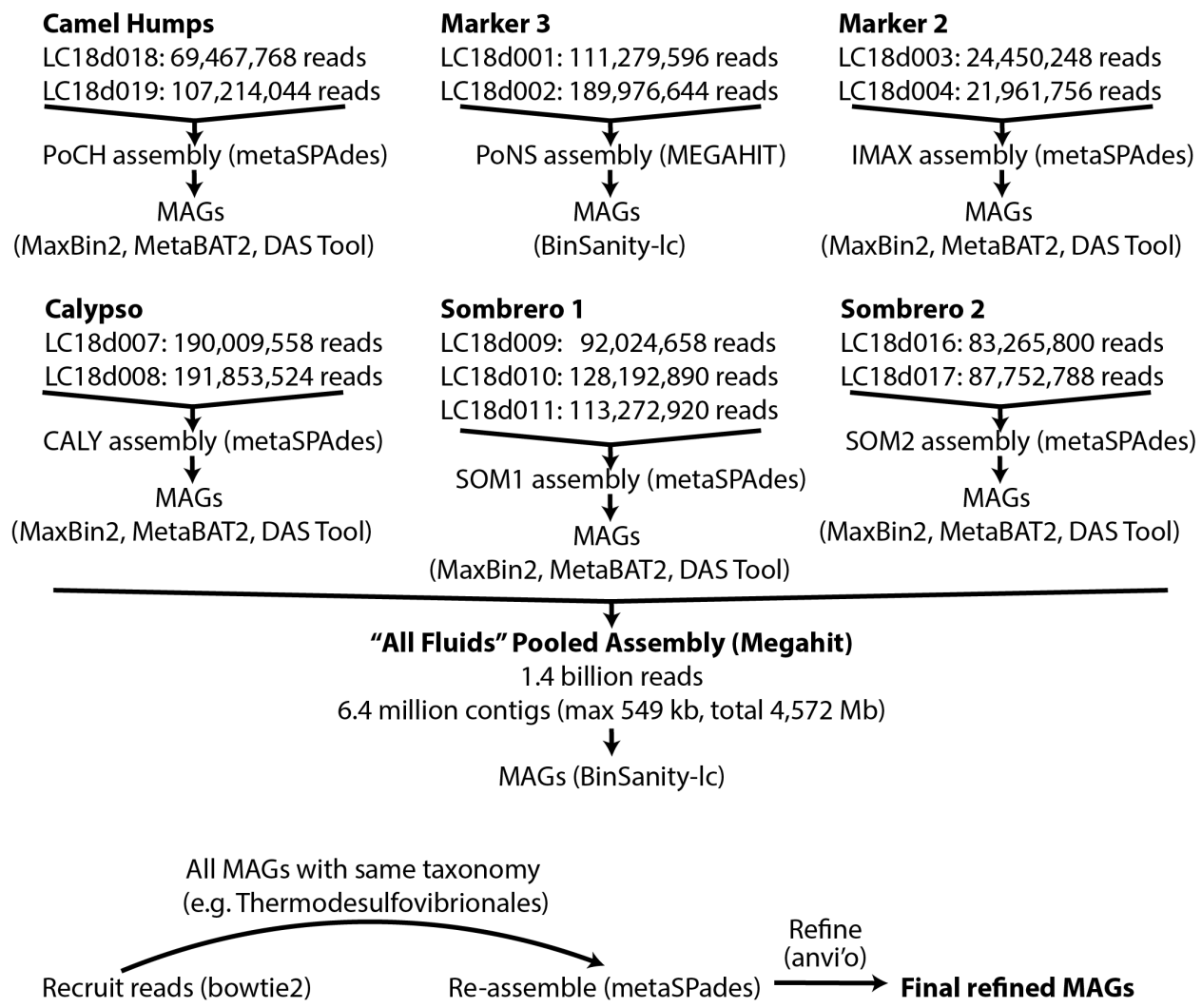
Sombrero 1



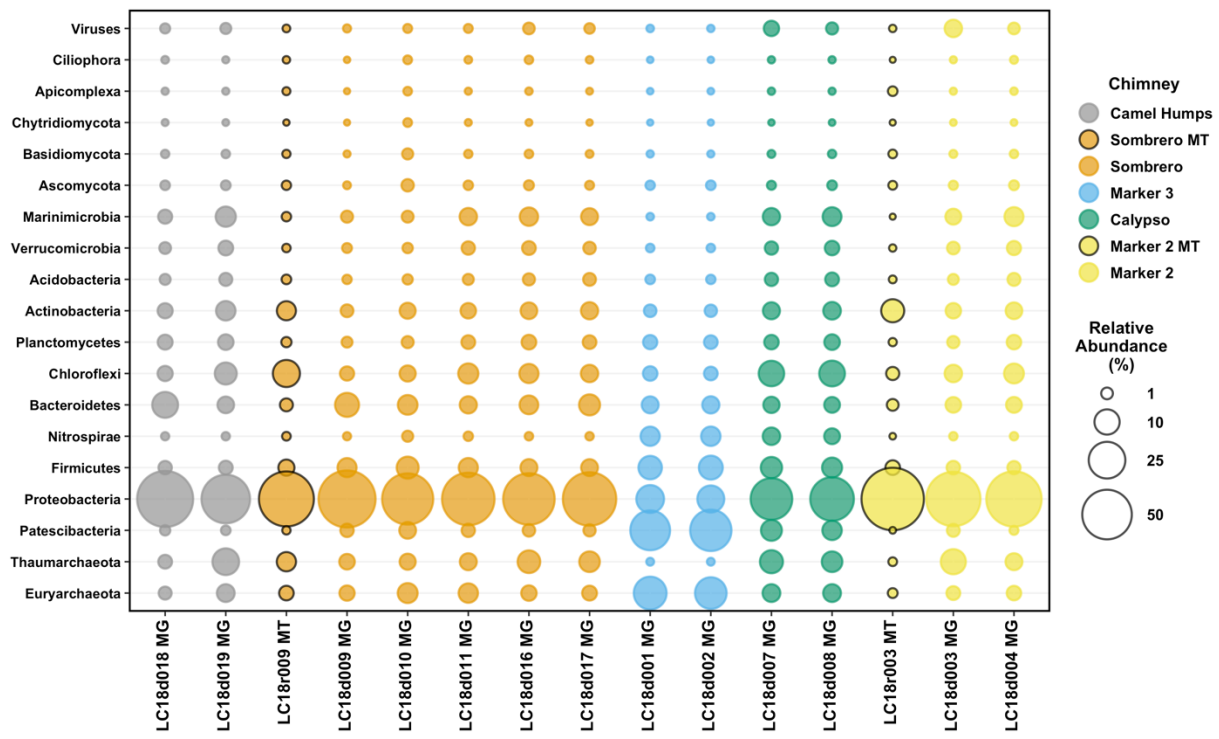
Sombrero 2



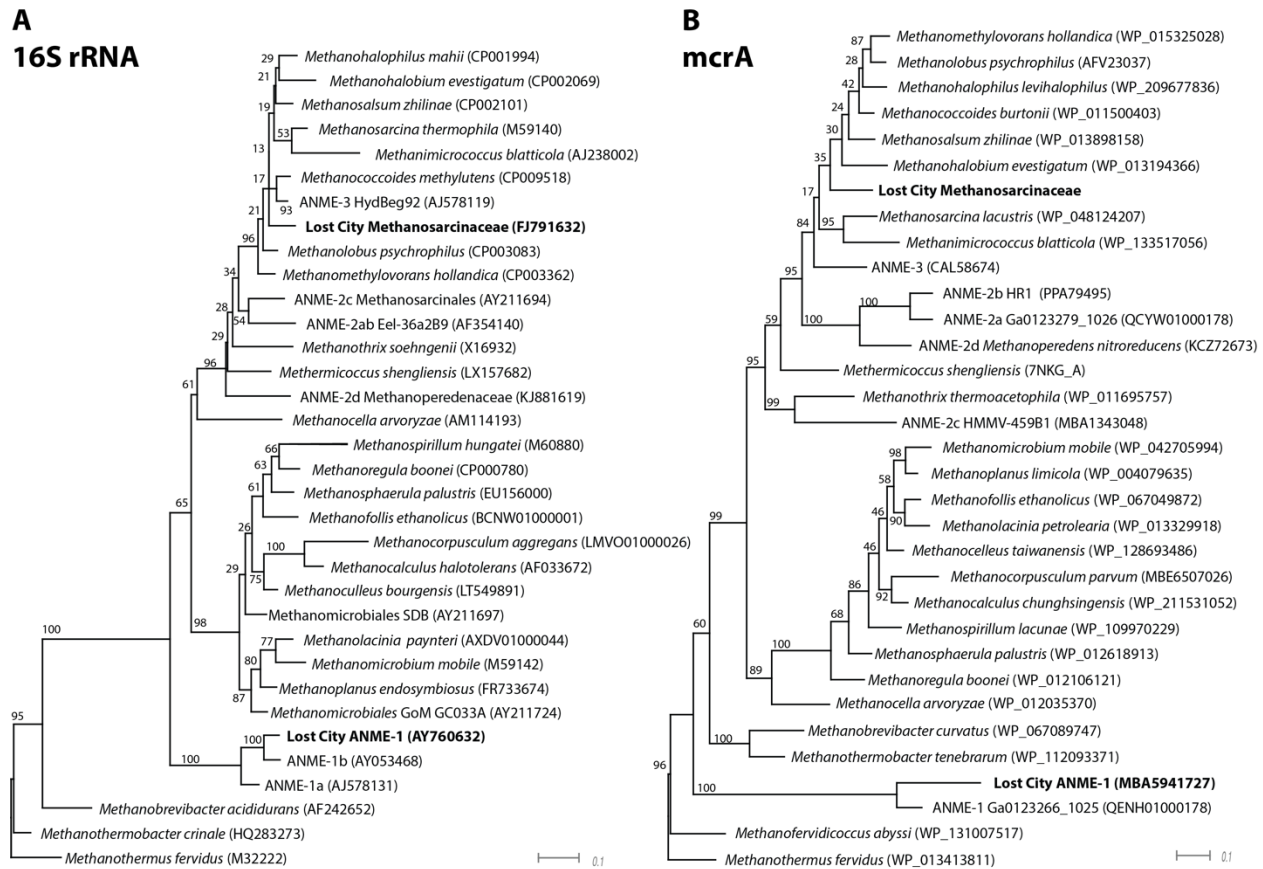
Supplemental Figure S2. Photographs of sampling locations for this study, captured on the seafloor by ROV *Jason*. Camel Humps and Marker 3 are visually distinct structures despite their nearby locations. Sombrero was sampled at the same location on two separate dives.



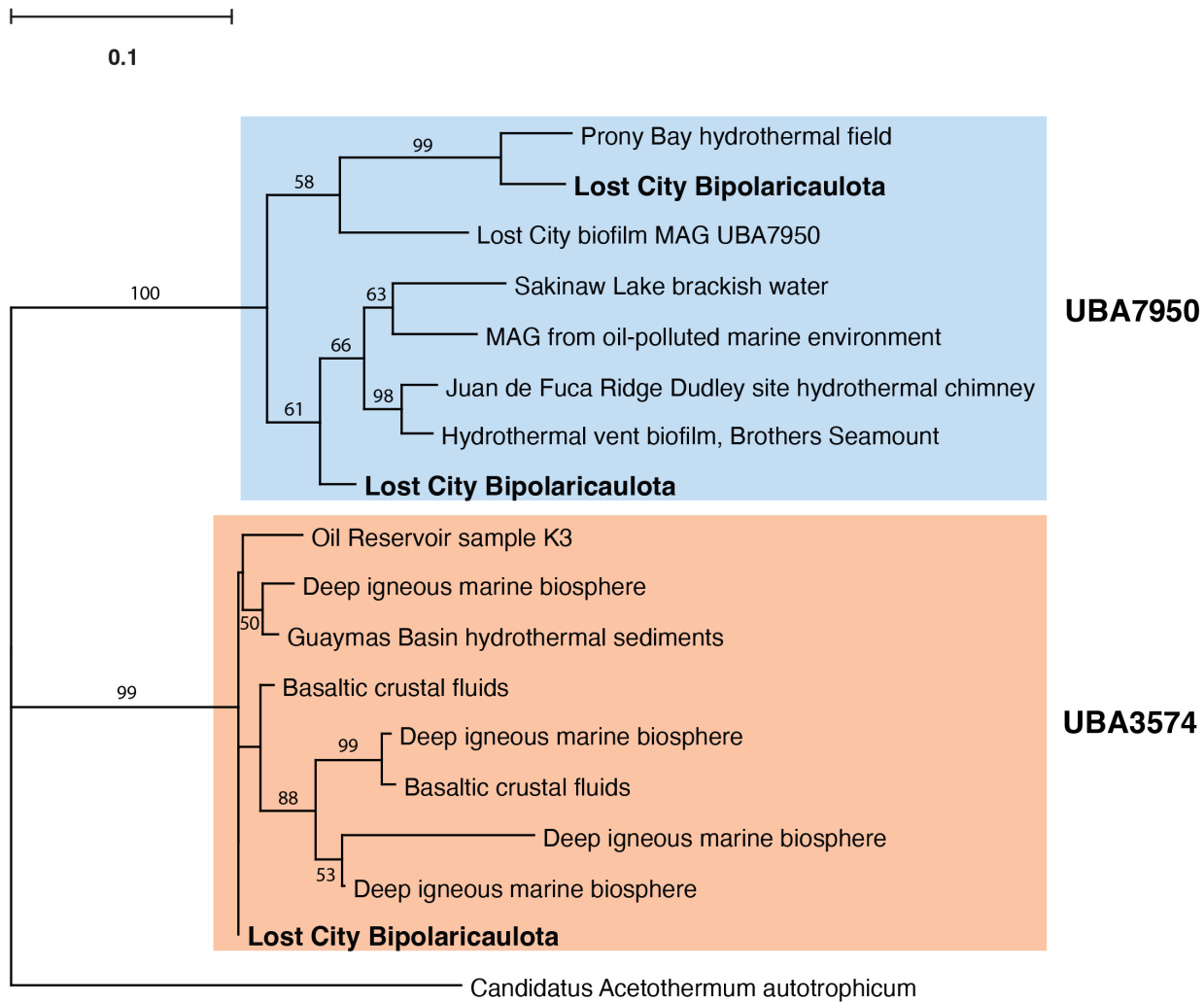
Supplemental Figure S3. Overall workflow for assembly of metagenomes and binning into metagenome-assembled genomes (MAGs). Assemblies were performed with reads pooled from each chimney location (chimney-specific assemblies), and one “all fluids” pooled assembly was performed with all metagenomic reads from all chimney locations. Initial bins constructed with automated tools were used as a template for recruiting metagenomic reads for a re-assembly and manual curation and refinement of the final MAGs.



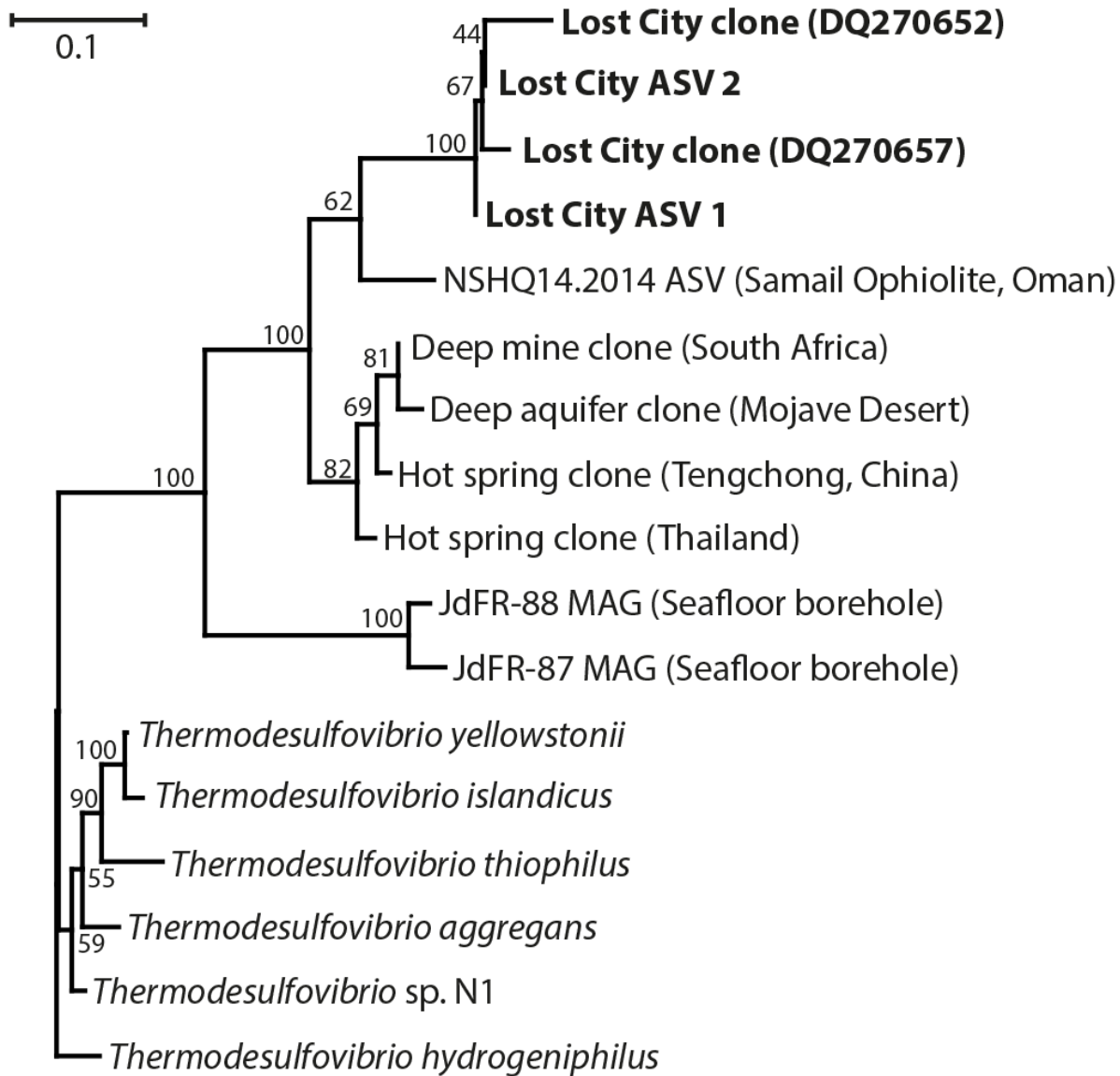
Supplemental Figure S4. Percent of reads classified to the top 18 phyla (plus viruses) in Lost City hydrothermal fluid samples. Unassembled reads were classified using Kaiju with its default NCBI nr+euk database. Percentages were calculated as the number of reads classified to each phyla divided by the total number of reads in that library that could be classified to the phylum level by Kaiju. Bubbles representing reads in metatranscriptomes (MT), rather than metagenomes (MG), are highlighted with black borders.



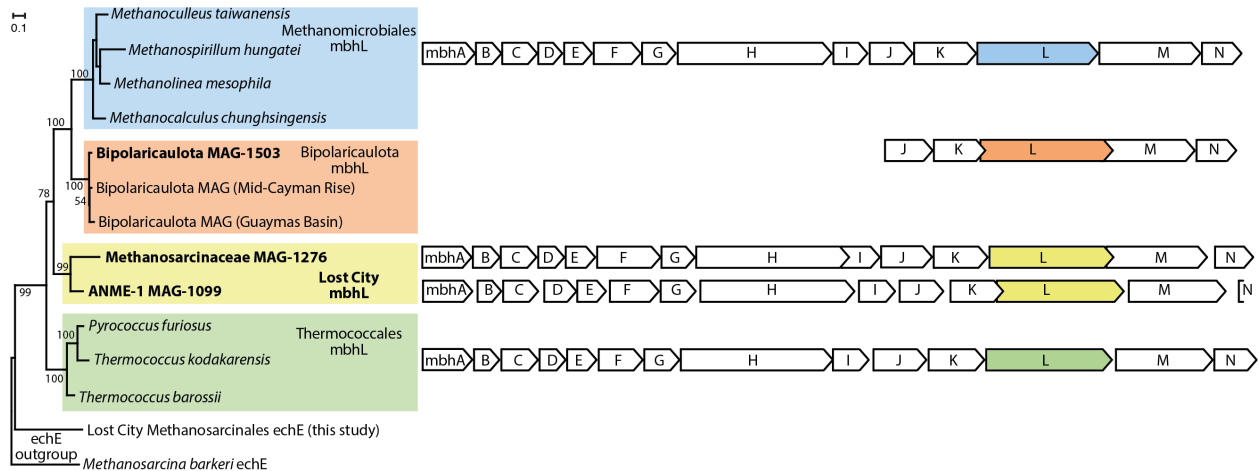
Supplemental Figure S5. Phylogenies of 16S rRNA and mcrA (alpha subunit of methyl coenzyme M reductase) highlighting Lost City MAGs classified as Methanosarcinaceae and ANME-1. Bootstrap support values are shown for each node. Sequences and accession IDs are provided in the Zenodo-archived GitHub repository accessible via DOI: 10.5281/zenodo.5798015.



Supplemental Figure S6. Phylogeny of 16S rRNA highlighting Lost City sequences classified as Bipolaricaulota. The most abundant Lost City Bipolaricaulota 16S rRNA sequences cluster into two distinct monophyletic groups, classified by GTDB as UBA3574 and UBA7950, which corresponds to the classifications of the three refined Bipolaricaulota MAGs (**Figure 3**). The UBA7950 sequences are further divided into two clades, one of which includes a MAG assembled by Parks et al. (2018) from our previous study of Lost City chimney biofilms (DOHL01000117). Bootstrap support values greater than 50 are shown for each node. Sequences and accession IDs are provided in the Zenodo-archived GitHub repository accessible via DOI: 10.5281/zenodo.5798015.

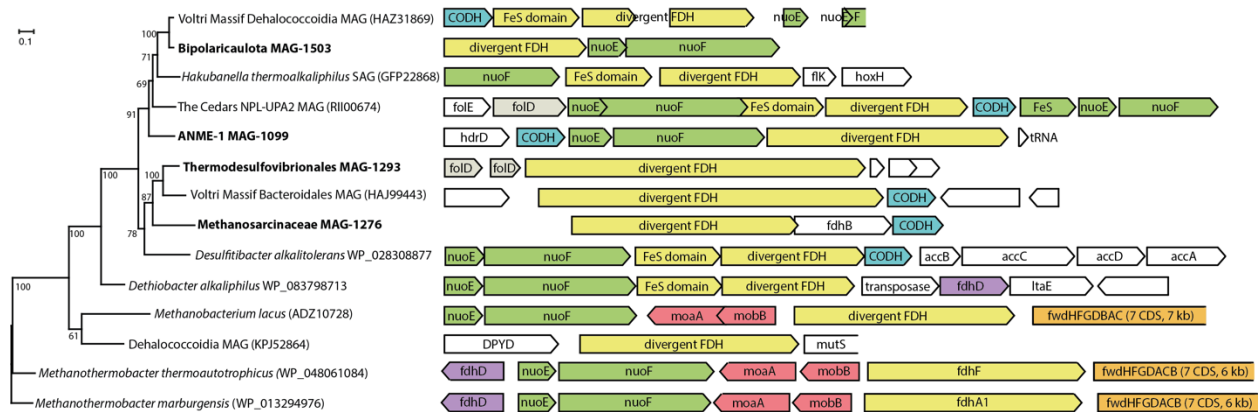


Supplemental Figure S7. Phylogeny of 16S rRNA highlighting Lost City sequences classified as *Thermodesulfovibrionia*. The two Lost City ASVs differ from each other by a single base and match sequences from a previously published clone library of Lost City chimney biofilms (Brazelton et al., 2006). They share 90% nucleotide identities with their closest neighbor, an ASV from alkaline borehole fluids in the Samail Ophiolite, Oman (Rempfert et al., 2017). Sequences and accession IDs are provided in the Zenodo-archived GitHub repository accessible via DOI: 10.5281/zenodo.5798015.



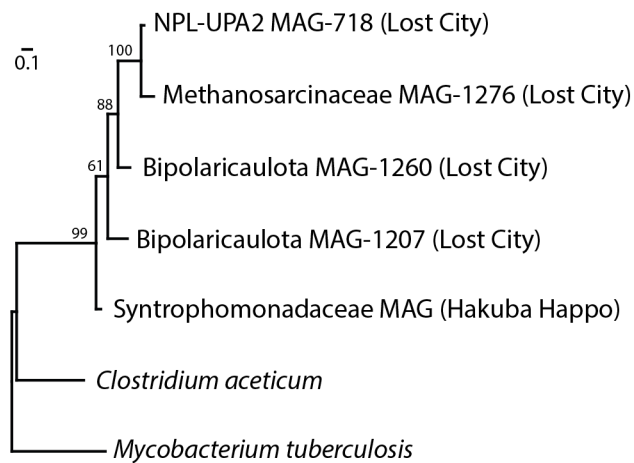
Supplemental Figure S8. Phylogeny of the large catalytic subunit of membrane-bound hydrogenase (mbhL) and the mbh gene cluster (expanded version of Figure 5).

Sequences and accession IDs are provided in the Zenodo-archived GitHub repository accessible via DOI: 10.5281/zenodo.5798015.

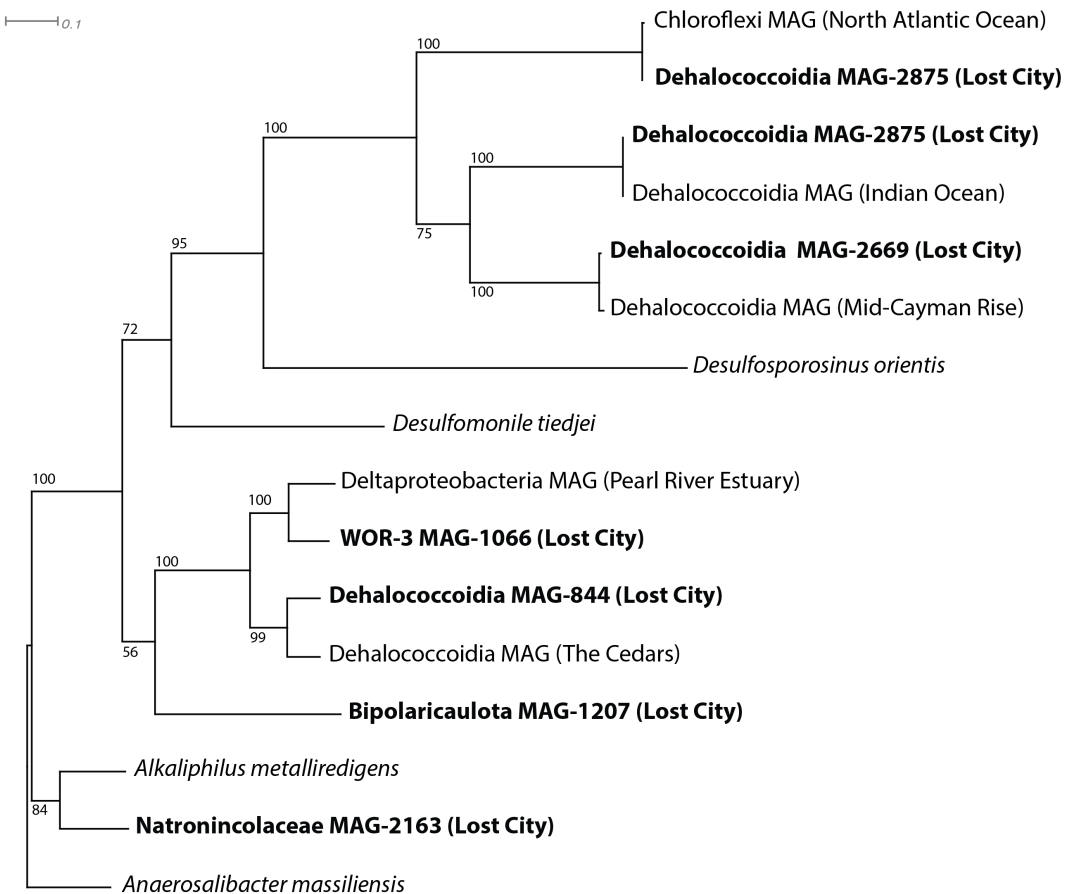


Supplemental Figure S9. Phylogeny of divergent FDH-like sequences (expanded version of Figure 6). In most cases, the divergent FDH-like gene was flanked by nuoEF (encoding NADH-quinone oxidoreductase) and a hypothetical sequence with a conserved domain associated with monomeric carbon monoxide dehydrogenase (CODH). Furthermore, most of these gene clusters contained signs of genome instability just upstream or downstream such as pseudogenes, transposases, or a toxin/antitoxin system (not shown here). Sequences and accession IDs are provided in the Zenodo-archived GitHub repository accessible via DOI:

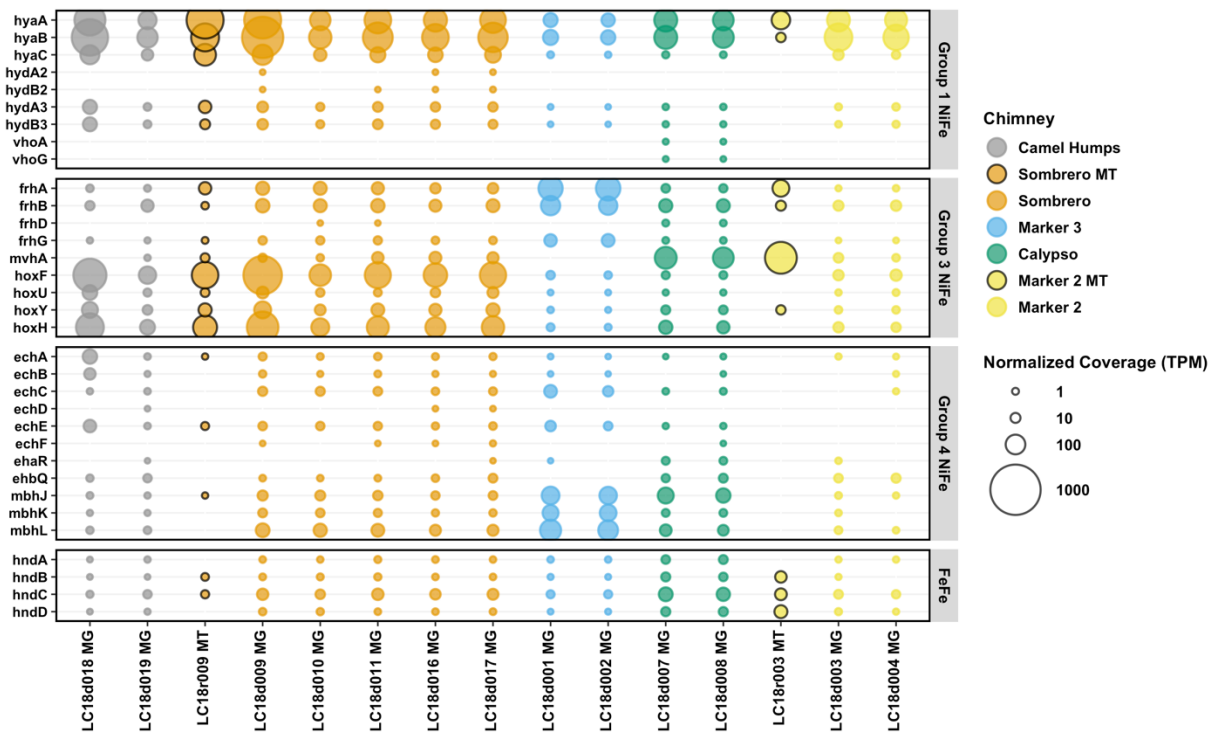
10.5281/zenodo.5798015.



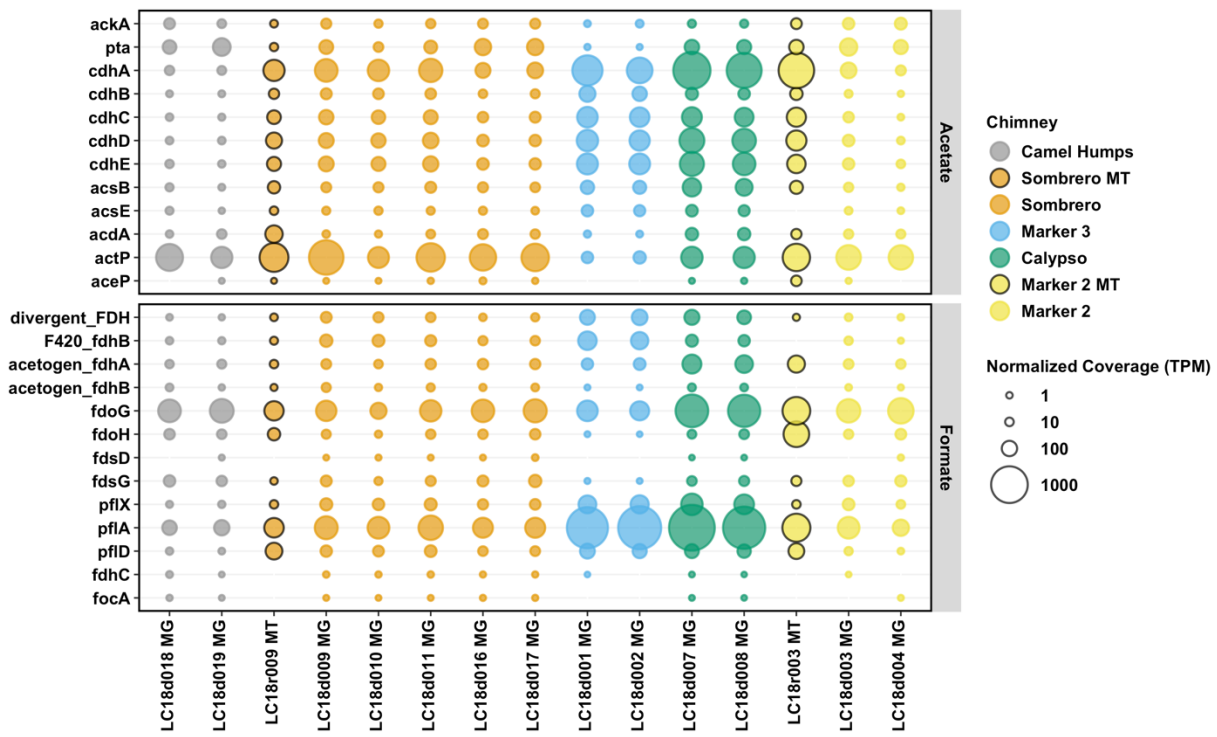
Supplemental Figure S10. Phylogeny of divergent sequences predicted to encode carbonic anhydrase. Lost City sequences form a novel clade including a predicted sequence from a MAG recovered from another serpentinite-hosted spring (Hakuba Happo). Bootstrap support values are shown for each node. Sequences and accession IDs are provided in the Zenodo-archived GitHub repository accessible via DOI: 10.5281/zenodo.5798015.



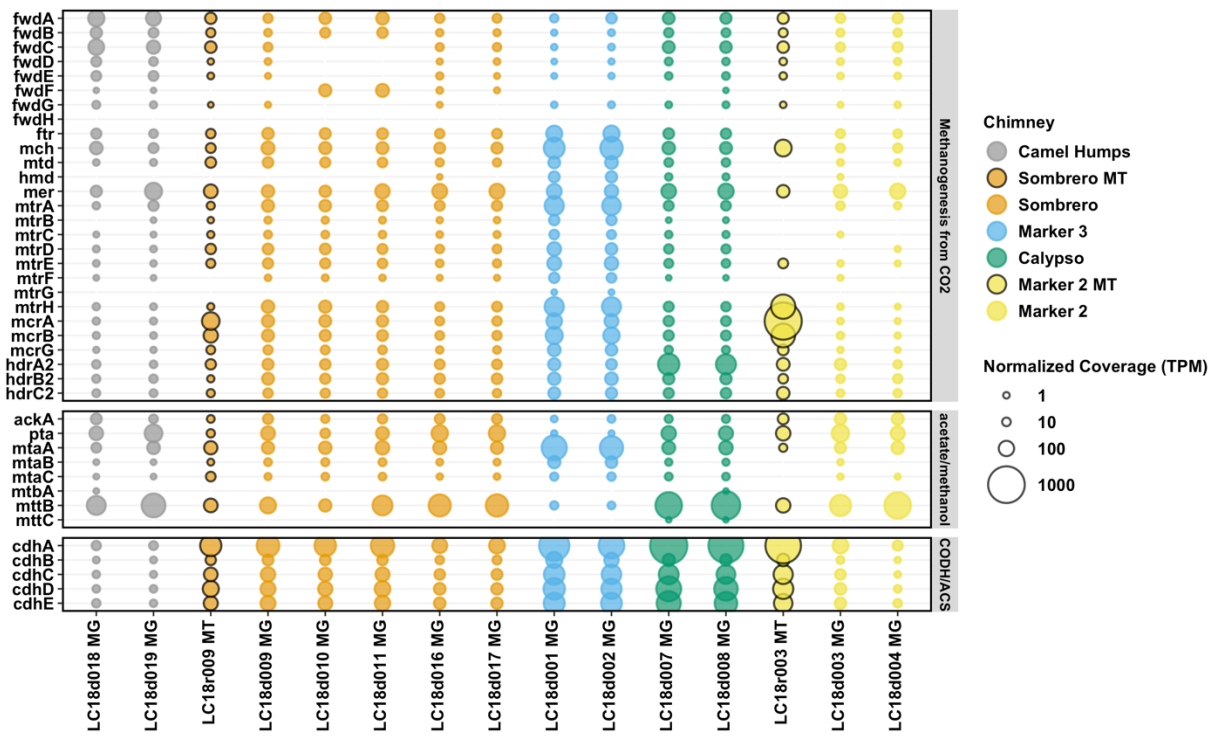
Supplemental Figure S11. Phylogeny of GrdB (beta subunit of glycine reductase). Lost City Bipolariculota, Dehalococcoidia, WOR-3, and Natronincolaceae MAGs share moderate sequence similarity (58-88% amino acid identities) with sequences from other MAGs (including one from another site of serpentinization, The Cedars), but limited similarity with sequences from characterized species. Lost City Dehalococcoidia MAGs that belong to the SAR202 marine cluster, including two copies from MAG-2875, form a separate clade from other Lost City MAGs that are more likely to represent subseafloor organisms. A second Natronincolaceae MAG not shown here lacks GrdB but includes all other genes associated with glycine reductase (**Supplemental Table S5**). Bootstrap support values are shown for each node. Sequences and accession IDs are provided in the Zenodo-archived GitHub repository accessible via DOI: 10.5281/zenodo.5798015.



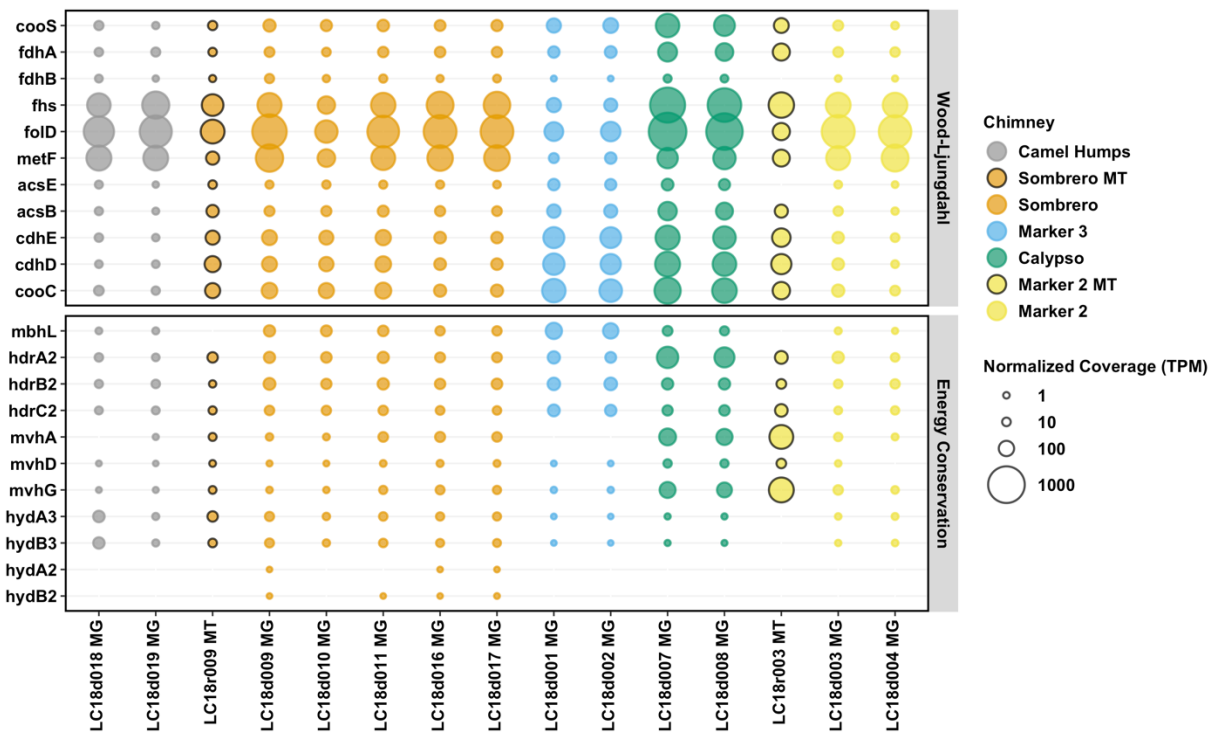
Supplemental Figure S12. Abundance of predicted hydrogenase sequences in Lost City hydrothermal fluid samples. Metagenomic coverage was normalized to predicted protein length and to the size of the metagenome or metatranscriptome library. The final normalized coverage is reported as a proportional unit (transcripts/fragments per million; TPM) suitable for cross-sample comparisons. Bubbles representing coverage in metatranscriptomes (MT), rather than metagenomes (MG), are highlighted with black borders. Genes are defined with KEGG Orthology; see **Supplemental Table S5**.



Supplemental Figure S13. Abundances of predicted sequences associated with acetate and formate metabolism in Lost City hydrothermal fluid samples. Metagenomic coverage was normalized to predicted protein length and to the size of the metagenome or metatranscriptome library. The final normalized coverage is reported as a proportional unit (transcripts/fragments per million; TPM) suitable for cross-sample comparisons. Bubbles representing coverage in metatranscriptomes (MT), rather than metagenomes (MG), are highlighted with black borders. Genes are defined with KEGG Orthology; see **Supplemental Table S5**.



Supplemental Figure S14. Abundance of predicted sequences associated with methanogenesis in Lost City hydrothermal fluid samples. Metagenomic coverage was normalized to predicted protein length and to the size of the metagenome or metatranscriptome library. The final normalized coverage is reported as a proportional unit (transcripts/fragments per million; TPM) suitable for cross-sample comparisons. Bubbles representing coverage in metatranscriptomes (MT), rather than metagenomes (MG), are highlighted with black borders. Genes are defined with KEGG Orthology; see **Supplemental Table S5**.



Supplemental Figure S15. Abundance of predicted sequences associated with acetogenesis in Lost City hydrothermal fluid samples. Metagenomic coverage was normalized to predicted protein length and to the size of the metagenome or metatranscriptome library. The final normalized coverage is reported as a proportional unit (transcripts/fragments per million; TPM) suitable for cross-sample comparisons. Bubbles representing coverage in metatranscriptomes (MT), rather than metagenomes (MG), are highlighted with black borders. Genes are defined with KEGG Orthology; see **Supplemental Table S5**.